INDIAN JOURNAL OF SCIENCE AND TECHNOLOGY

RESEARCH ARTICLE

Impacts of Thermal Radiation and Viscous Dissipation on the Boundary Layer Flow of Ferrofluid Past a Non-Flat Stretching Sheet in a Permeable Medium: Darcy-Forchheimer's Model

Sushil Prasad[1]*, **Shilpa Sood**[2], **Shikha Chandel**[3], **Diksha Sharma**[3]

1 Research Scholar, Mathematics & Statistics, Career Point University, Hamirpur, Himachal Pradesh, India
2 Associate Professor, Mathematics & Statistics, Career Point University, Hamirpur, Himachal Pradesh, India
3 Assistant Professor, Mathematics & Statistics, Career Point University, Hamirpur, Himachal Pradesh, India

OPEN ACCESS

Received: 27-11-2023
Accepted: 07-02-2024
Published: 29-02-2024

Citation: Prasad S, Sood S, Chandel S, Sharma D (2024) Impacts of Thermal Radiation and Viscous Dissipation on the Boundary Layer Flow of Ferrofluid Past a Non-Flat Stretching Sheet in a Permeable Medium: Darcy-Forchheimer's Model. Indian Journal of Science and Technology 17(11): 990-1002. https://doi.org/10.17485/IJST/v17i11.3027

* **Corresponding author**.

sushilprasad47@gmail.com

Funding: None

Competing Interests: None

Published By Indian Society for Education and Environment (iSee)

ISSN
Print: 0974-6846
Electronic: 0974-5645

Abstract

Objectives: The current research explores the impacts of thermal radiation and viscous dissipation on MHD ferrofluid boundary layer flow past a non-flat stretching sheet in a permeable medium utilizing a Darcy-Forchheimer model. **Methods:** Magnetite nanoparticles (Fe_3O_4) disintegrate in base fluids using the Tiwari-Das model of nanofluids. The governing partial differential equations are transformed into nonlinear ordinary differential equations (ODEs) using the relevant similarity variables. These nonlinear ODEs are solved numerically using the bvp4c- technique in MATLAB software. The effects of pertinent parameters such as the magnetic parameter, porosity parameter, Forchheimer parameter, Prandtl number, Eckert number, and radiation parameter on velocity and temperature fields are plotted graphically. The influence of physical factors on Skin friction coefficient and local Nusselt number are computed and examined. **Findings:** An augmentation in values of porosity parameter (λ), magnetic field (M), and Forchheimer number (Fr) reduce the momentum boundary layer thickness although increases the thermal boundary layer thickness. An increase in the fluid's temperature is due to an increase either in the radiation parameter (Rd) or in the Eckert number (Ec). Escalation in Prandtl number (Pr) lowers the compactness of the thermal boundary layer. **Novelty:** The current work focuses on the innovative investigation of the impact of heat radiation and viscous dissipation on the boundary layer flow of MHD ferrofluid via a stretched sheet with varying thickness and no research on the topic covered in this article has yet to be reported. The study also incorporates the use of the Darcy-Forchheimer model. Here, water (H_2O) is used as the base fluid, and magnetite (Fe_3O_4) is used as nanoparticles for the present study. The results coincide very well with previous

published works that authenticate the validity of the current work.

Keywords: Ferrofluid; MHD; Stretching sheet with variable thickness; Thermal radiation; Viscous dissipation

1 Introduction

The necessity of enhancing heat transmission in industrial applications has gained significant focus in the past few decades. Pure fluids comprising water, oil, and ethylene can be used as cooling liquids in most applications. The heat transmission rates of these fluids are nevertheless inadequate. The dispersion of nanoscale particles into the base fluid improves its thermal performance and rate of heat transmission. Thermal conductivity and heat transmission are greatly enhanced when nanoparticles are incorporated into the base fluid. Since the completion of this study, nanofluids have found widespread use in power production, heating and cooling systems, nuclear applications, medical, electronics, automotive, and other fields [(1)].

A magnetic force is applied to synthetic fluids called ferrofluids. These liquids consist of magnetic particles with a diameter that varies from 5 to 15 nm, suspended in colloidal suspensions that are chemically stable. The aforementioned fluids may also be referred to as magnetic nanofluids due to the diameter and size of the magnetised particles. Ferrofluids increase a fluid's thermal characteristics by acting like nanoparticles. A magnetic field affects the temperature distribution and other physical properties of ferrofluids. Due to this characteristic, ferrofluids are significantly more useful in a variety of fields, including engineering and biological sciences. These fluids exhibit properties similar to those of ordinary liquids in the absence of magnetic force. In today's technological and chemical sectors, ferromagnetic fluids find amazing applications. These liquids are employed in some commercially available electromechanical devices, such as electric engines, transformers, hard discs, electromagnets, generators, and rotating X-ray tubes. They are also employed in the biological sciences to treat hoarding, which is the process of keeping records and hard plates [(2)].

In multiple fields of astronomy, engineering, geophysics, and aerospace engineering, magneto-hydrodynamic phenomena are extensively exploited. Examples include heat exchangers, electromagnetic casting, photochemical reactors, sensors, transport, fibre coating, magnetic drug targeting, cooling nuclear reactors, and so on. A recent study by Abbas et al. [(3)] looked into how MHD axisymmetric micropolar nanofluid flows through porous parallel discs. They found that the radial velocity curves get steeper near the discs and flatter in the middle. Rauf et al. [(4)] looked at how heat flux and Cattaneo-Christov mass affect three-dimensional MHD fluid flows across an oscillating disc. They implemented the sequential over-relaxation (SOR) approach in conjunction with finite difference discretization to resolve highly nonlinear ODEs. Ullah et al. [(5)] explored the significance of thermal density and viscous dissipation on heat and mass transfer of chemically reactive nanofluid flow along stretching sheet under magnetic field. Shah et al. [(6)] examined the effect of thermal radiation on convective heat transfer in MHD boundary layer Carreau fluid with chemical reaction.

It is extremely easy to make assumptions about fluid flowing through a porous medium. Since the universe's formation, we have been surrounded by incredibly realistic scenarios, such as fluids naturally flowing via sand and dusty places or through a stony surface. These days, this principle is frequently applied in the manufacturing sector for a variety of reasons, particularly when modelling oil reservoirs, groundwater management systems, geothermal engineering, and many related fields as well. While the traditional Darcy rule aroused close attention, it was only applicable in very specific cases where the porosity factor was kept low. It does not account for the increased rate of fluid momentum passing through the porous medium. Therefore, to increase its

application, the traditional Darcy law demands that it be modified. To deal with the higher porosity rates, Forchheimer added the squared velocity factor to the momentum equation of the model that governs the classical Darcy law. A lot of different technical, environmental, and industrial settings use porous materials for convection. These include geological setups, geothermic systems, chemical action reactors, and heat exchangers. The Darcy-Forchheimer model encompasses mechanical phenomena, drag forces, and diffusion effects. The model is utilised in fluid flow as well as heat flux analysis to investigate mechanical phenomena. The heat transfer phenomena in nanofluids flowing across composite porous media were studied by Hemavathi and Umavathi [7]. Aleem et al. [8] revealed the characteristics of Newtonian heating as well as the chemical reaction occurring in a nanofluid flowing across a Darcy medium.

The impacts of thermal radiation on our industrial and technological fields are significant. Procedures are carried out at extremely high temperatures in various non-isothermal circumstances and situations where heat transfer coefficients for convection are smaller. The radiative flux of heat is quantified by the Rosseland approximation for the analysis of heat convection. Practical applications for radiative heat transfer may be encountered in spacecraft, nuclear reactors, gas turbines, nuclear power plants, supersonic flight, nuclear power plants, and other essential equipment. Employing a Forchheimer porous medium, Bejawada et al. [9] examined the radiation impact on MHD Casson fluid flow across an inclined, non-linear surface with a chemical reaction. The temperature of the plate was seen to decline when the radiation parameter and Forchheimer porous media parameter values increased. It is anticipated that the temperature distribution of the nanofluid will improve with increasing estimates of nanoparticle concentrations and radiation parameters, according to Hussain et al.'s [10] evaluation of the convection analysis of the radiative nanofluid flow via porous media across a stretching surface beneath an inclined magnetic field.

These days, researchers concentrate on researching the consequences of heat and mass transmission that may be used to enhance the thermal properties of fluids. This is because fluid thermal features play a major role in many flow assessments of computational fluid mechanics. Viscous dissipation and radiant heat are two elements that are essential for enhancing thermal properties. The system's proper temperature is produced via viscous dissipation, which also serves as a heat source. When a fluid moves and overwhelms the layers of shear forces, it produces heat via an irreversible process known as viscous dissipation [11]. By taking into account viscous dissipation and magneto-hydrodynamics, Khashi et al. [12] scrutinised the radiated heat transfer and studied the fluid model of Reiner-Philippoff flowing across a nonlinearly shrinkable sheet. Saidulu and Reddy [13] looked at the implications of dissipation on the propagation of mass and heat by analysing micropolar flow on a stretchable surface. Their conclusion showed that the concentration curve decreased with increasing Schmidt number inputs, but the temperature curve increased for higher values of Eckert number.

So far as we are aware, no studies have been published on the topic that is discussed in this article. So, this is an innovative way of unravelling the impacts of thermal radiation and viscous dissipation on the boundary layer flow of MHD ferrofluid past a stretching sheet with variable thickness utilising the Darcy-Forchheimer model. As a result, the current numerical analysis has been performed to fill this gap. The paired partial differential equations that are non-linear can be transformed into a set of paired ordinary differential equations that are non-linear. The altered equations are resolved numerically by the bvp-4C method. Graphs of several important physically integrated parameters are created using the velocity and temperature fields' graphical representations. Tables serve to quantitatively determine the relevant physical quantities, such as the coefficient of local skin friction along with local Nusselt numbers.

2 Methodology

This section considers a steady, incompressible, two dimensional (x, y) laminar flow past a stretching sheet along with variable thickness (Figure 1) via Darcy-Forchheimer's relation in the existence of magnetic field, thermal radiation, and viscous dissipation effects. The sheets are placed towards the $x-$ axis and is stretched with velocity $U_w(\mathrm{x}) = U_o(x+b)^m$, where U_o & b are the dimensional constants and m refers to velocity power index. The stretching surface is chosen along the direction of the flow while $y-$ axis is orthogonal to it. T_w denotes temperature of fluid placed near to wall, T_∞ signifies the ambient temperature and B represents transverse magnetic field. The thickness varied significantly as $y = A(x+b)^{\frac{1-m}{2}}$ where A is relatively small constant indicating that the sheet cannot be flat and sufficiently thin. The sheet becomes flattens when $m = 1$.

2.1 Governing Equations

The basic boundary layer equations for the aforementioned model in Cartesian coordinates x and y are as follows: (see [14])

$$\frac{\partial u}{\partial x} + \frac{\partial v}{\partial y} = 0, \tag{1}$$

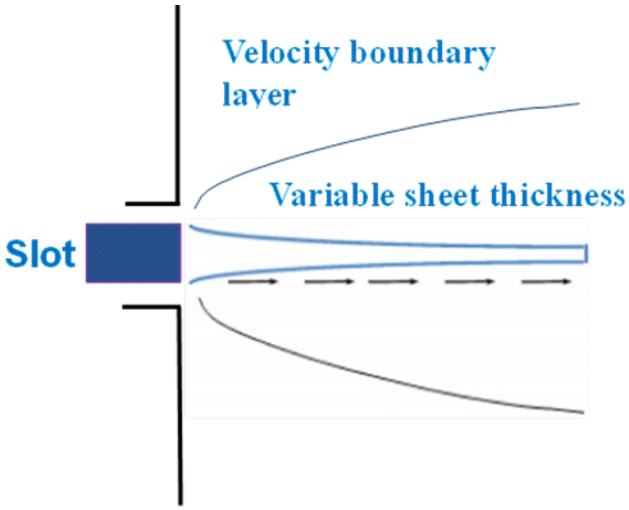

Fig 1. Physical description of a stretching sheet with variable thickness

$$u\frac{\partial y}{\partial x}+v\frac{\partial u}{\partial y}=U_\infty\frac{dU_\infty}{dx}+\frac{\mu_{nf}}{\rho_{nf}}\frac{\partial^2 u}{\partial y^2}-\frac{\sigma_{nf}}{\rho_{nf}}B^2(x)(u-U_\infty)-\frac{\nu_{hnf}}{k}(u-U_\infty)+\frac{F}{\rho_{nf}}(U_\infty^2-u^2), \tag{2}$$

$$u\frac{\partial T}{\partial x}+v\frac{\partial T}{\partial y}=\frac{k_{nf}}{(\rho C_p)_{nf}}\frac{\partial^2 T}{\partial y^2}-\frac{1}{(\rho C_p)_{nf}}\frac{\partial q_r}{\partial y}+\frac{\mu_{nf}}{(\rho C_p)_{nf}}\left(\frac{\partial u}{\partial y}\right)^2. \tag{3}$$

where (u,v) represents velocity components of fluid along (x,y) directions, respectively. T denotes the temperature, B is the induced magnetic field, which should be very minimal in compared to the applied magnetic field and is omitted. ρ_{nf} represents the density, μ_{nf} refers the dynamic viscosity, σ_{nf} depicts electrical conductivity, $(\rho C_p)_{nf}$ represents the heat capacitance, k_{nf} denotes the thermal conductivity of nanofluid, q_r indicates radiative heat.

The Rosseland approximation [15] being used to evaluate and simply the radioactive heating flux in the temperature equation, i.e.

$$q_r=-\frac{4\sigma^*}{3K^*}\frac{\partial T^4}{\partial y}, \tag{4}$$

Here, σ^* & K^* represents Stefan-Boltzman constant and mean absorption co-efficient, respectively. It is anticipated that variations in temperature throughout the flow are expected to be minimal, with this in mind, the factor T^4 can be expressed as a linear function of the temperature ignoring the higher order terms, whereas T^4 can be expanded in Taylor's series about T_∞ which is derived thereby,

$$T^4=T_\infty^4+4T_\infty^3(T-T_\infty)^2+6T_\infty^2(T-T_\infty)^2+\ldots\ldots\ldots\ldots \tag{5}$$

By omitting the higher order terms of previously stated assertion beyond the first degree in the series:

$$T^4\approx 4TT_\infty^3-3T_\infty^4 \tag{6}$$

Now,

$$q_r=-\frac{16\sigma^*T_\infty^3}{3K^*}\frac{\partial T}{\partial y}. \tag{7}$$

Using Equation (7), the energy Equation (3) be reduced to

$$u\frac{\partial T}{\partial x}+v\frac{\partial T}{\partial y}=\frac{k_{nf}}{(\rho C_p)_{nf}}\frac{\partial^2 T}{\partial y^2}+\frac{1}{(\rho C_p)_{nf}}\frac{16\sigma^*T_\infty^3}{3K^*}\frac{\partial^2 T}{\partial y^2}+\frac{\mu_{nf}}{(\rho C_p)_{nf}}\left(\frac{\partial u}{\partial y}\right)^2. \tag{8}$$

2.2 Boundary conditions

The boundary constraints for the subjected problem are given by (see[16])

$$\begin{aligned} u=\ U_w(x)=U_o(x+b)^m,\ v=0,\ T=\ T_w(x) \qquad & at\ y=A(x+b)^{\frac{1-m}{2}},\\ u=\ U_\infty(x)=U_1(x+b)^m,\ T\to\ T_\infty \qquad & as\ y\to\infty, \end{aligned} \tag{9}$$

where $T_w(x)=T_\infty+T_o(x+b)^{\frac{m-1}{2}}$ denotes the temperature near to wall, T_∞ is the temperature far-off from the wall, $B(x)=B_o(x+b)^{\frac{m-1}{2}}$ is the induced magnetic field and $U_\infty(x)=\ U_1(x+b)^{\frac{m-1}{2}}$.

2.3 Similarity Transformations

The similarity transmutations have been invoked following[17], given as:

$$\begin{aligned} &\psi=F(\eta)\sqrt{\frac{2}{m+1}\nu_f U_{o(x+b)}}^{\frac{m+1}{2}},\ \eta=y\sqrt{\frac{m+1}{2}\frac{U_o}{\nu_f}}_{(x+b)}^{\frac{m-1}{2}},\ \Theta(\eta)=\frac{T-T_\infty}{T_w-T_\infty},\\ &u=U_o(x+b)^m f'(\eta),\ v=-\sqrt{\frac{m+1}{2}\nu_f U_o}_{(x+b)}^{\frac{m-1}{2}}\left[f(\eta)+\eta\frac{m-1}{m+1}f'(\eta)\right]. \end{aligned} \tag{10}$$

Here ψ, ν_f, & η represents stream function, kinematic viscosity, & similarity variable, whereas F & Θ are the function of η.

2.4 Transformed equations

Next, we define $u=\frac{\partial\psi}{\partial y}$, $v=-\frac{\partial\psi}{\partial x}$. Equation (1) is being automatically satisfied whereas by employing Equation (10), rest of Equations (2) and (3) be transformed as

$$\frac{\mu_{nf}/\mu_f}{\rho_{nf}/\rho_f}F'''+FF''-\frac{2m}{m+1}\left(F'^2-\varepsilon^2\right)-\frac{\sigma_{nf}/\sigma_f}{\rho_{nf}/\rho_f}M\left(F'-\varepsilon\right)-\frac{\mu_{nf}/\mu_f}{\rho_{nf}/\rho_f}\lambda\left(F'-\varepsilon\right)-\frac{1}{\rho_{nf}/\rho_f}Fr(F'^2-\varepsilon^2)=0 \tag{11}$$

$$\left(\frac{k_{nf}}{k_f}+\frac{4}{3}Rd\right)\Theta''+Pr\left(\frac{(\rho C_p)_{nf}}{(\rho C_p)_f}F\Theta'+\frac{\mu_{nf}}{\mu_f}EcF''^2\right)=0. \tag{12}$$

2.5 Transformed boundary conditions

The transformed boundary conditions (Equation (9)) are:

$$\begin{aligned} &F(\eta)=\alpha\left(\frac{1-m}{1+m}\right),\ F'(\eta)=1,\ \Theta(\eta)=1 \qquad at\ \eta=0,\\ &F'(\eta)=\varepsilon,\ \Theta(\eta)=0 \qquad as\ \eta\to\infty. \end{aligned} \tag{13}$$

Here, $(')$ denotes derivatives with respect to η, and $\alpha=A\sqrt{\frac{m+1}{2}\frac{U_o}{\nu_f}}$. Supposing and substituting $F(\eta)=f(\eta-\alpha)=f(\zeta)$, and $\Theta(\eta)=\theta(\eta-\alpha)=\theta(\zeta)$, we get:

$$\frac{\mu_{nf}/\mu_f}{\rho_{nf}/\rho_f}f'''+ff''-\frac{2m}{m+1}\left(f'^2-\varepsilon^2\right)-\frac{\sigma_{nf}/\sigma_f}{\rho_{nf}/\rho_f}M\left(f'-\varepsilon\right)-\frac{\mu_{nf}/\mu_f}{\rho_{nf}/\rho_f}\lambda\left(f'-\varepsilon\right)-\frac{1}{\rho_{nf}/\rho_f}Fr(f'^2-\varepsilon^2)=0, \tag{14}$$

$$\left(\frac{k_{nf}}{k_f}+\frac{4}{3}Rd\right)\theta''+Pr\left(\frac{(\rho C_p)_{nf}}{(\rho C_p)_f}f\theta'+\frac{\mu_{nf}}{\mu_f}Ecf''^2\right)=0. \tag{15}$$

and the reduced BCs are:

$$\begin{aligned} &f(\zeta)=\alpha\left(\frac{1-m}{1+m}\right),\ f'(\zeta)=1,\ \theta(\zeta)=1 \qquad at\ \zeta=0,\\ &f'(\zeta)=\varepsilon,\ \theta(\zeta)=0 \qquad\qquad\qquad as\ \zeta\to\infty. \end{aligned} \tag{16}$$

where, $(')$ signifies differentiation w.r.t. ζ and the dimensionless parameters i.e., M, ε, λ, Fr, Pr, Ec, Rd, α are the magnetic field, velocity ratio parameter, porosity parameter, forchheimer no., Prandtl no., Eckert no., radiation parameter and wall thickness parameter respectively. The expressions, for these parameters are as given below:

$$M=\frac{2\sigma_o B_o^2}{\rho_f U_o(m+1)},\ \varepsilon=\frac{U_1}{U_o},\ \lambda=\frac{2\nu_f(x+b)^{1-m}}{kU_o(m+1)},\ Fr=\frac{2F(x+b)}{\rho_f(m+1)},\ Pr=\frac{\nu_f}{\alpha_f},$$
$$Ec=\frac{U_w^2}{(C_p)_f(T_w-T_\infty)},\ Rd=\frac{16\sigma^* T_\infty^3}{3k_f K^*},\ \alpha=A\sqrt{\frac{m+1}{2}\frac{U_o}{\nu_f}}.$$

Table 1. Thermophysical properties of magnetic nanoparticles & base fluid [18]

Physical properties	Fe_3O_4	Water
$\rho(kg/m^3)$	5180	997.1
$C_p(J/kg.K)$	670	4179
$k(W/m.K)$	9.7	0.613
$\beta(K^{-1})$	1.3 x 10^{-5}	21
$\mu(mPa/s)$	-	0.891
Pr	-	6.2

Table 2. Thermophysical properties of nanofluid [19]

Properties	Nanofluid
Density	$\rho_{nf}=(1-\phi)\rho_f+\phi\rho_s$
Heat Capacity	$(\rho C_p)_{nf}=(1-\phi)(\rho C_p)_f+\phi_1(\rho C_p)_s$
Thermal Conductivity	$k_{nf}=\frac{k_s+2k_f-2\phi\left(k_f-k_s\right)}{k_s+2k_f+\phi\left(k_f-k_s\right)}k_f$
Electrical Conductivity	$\sigma_{nf}=(1-\phi)\sigma_f+\phi\sigma_s$
Dynamic viscosity	$\mu_{nf}=\frac{\mu_f}{(1-\phi)^{2.5}}$

- **Parameters of empirical importance**

Coefficient of local Skin friction & local Nusselt number is defined as:

$C_f=\frac{\tau_w}{\rho_f U_w^2(x)}, Nu=\frac{(x+b)q_w}{k_f(T_w-T_\infty)}$,

where τ_w represents the shear stress through surface of the wall & q_w gives the heat flux against the wall. These terms are listed as:

$\tau_w=\mu_{nf}\left(\frac{\partial u}{\partial y}\right)_{y=0}$, and $q_w=-\left[k_{nf}+\frac{16\sigma^* T_\infty^3}{3K^*}\right]\left(\frac{\partial T}{\partial y}\right)_{y=0}$.

Upon imposing the similarity transformations and dominated boundary conditions, the coefficient of local Skin friction and local Nusselt number are stated in non-dimensional formats as:

$C_{fx}=C_f(Re_x)^{\frac{1}{2}}=\frac{\mu_{hnf}}{\mu_f}\sqrt{\frac{m+1}{2}}\left(f''(\eta)\right)_{\eta=0}$,

$Nu_x(Re_x/2)^{-\frac{1}{2}}=-\left(\frac{k_{hnf}}{k_f}+\frac{4}{3}Rd\right)\sqrt{\frac{m+1}{2}}\left(\theta'(\eta)\right)_{\eta=0}$,

where $Re_x=\frac{U_w(x+b)}{\nu_f}$ denotes the Reynold's number.

- **Utilization of the bvp4c solver**

For the purpose of solving BVPs, MATLAB has a method that may be used. It was Kierzenka and Shampine[20] who were the pioneers in the design and implementation of the bvp4c solver. They are now demonstrating a significant amount of study on the subject[21]. According to this research, an analysis of the interpretative implementation of bvp4c for the study that is now being considered has been carried out. In order to calculate this arrangement, we first changed the entity of PDEs to the entity of ODEs by utilizing similarity transformations. After that, we utilized the bvp4c solver that is available in MATLAB. Subsequently, we transform the entity of ordinary differential equations (ODEs) into an entity of first-order equations. Furthermore, the bvp4c approach may be utilized to design solutions for any issue that is associated with boundaries. In order to illustrate the procedure, Shampine has produced a demonstration. The transformation of the entity of ODEs for the purpose of the current research into the entity of first-degree equations has been investigated in Steps I and II that have been completed. Step III is where the boundary condition conversion is handled, and step IV is where the remaining section of the program is completed.

Step I: Firstly, we introduce a distinct set of variables for our paired non-linear ODEs:

$$f(1) = f,\ f(2) = f^{'},\ f(3) = f^{''},\ f(4) = \theta,\ f(5) = \theta'$$

Step II: Now, we add new variables to a set of equation & construct a structure of 1st order equation as:

$$f'(1) = f(2)$$
$$f'(2) = f(3)$$
$$f'(3) = \frac{\rho_{nf}/\rho_f}{\mu_{nf}/\mu_f}\left(-ff'' + \frac{2m}{m+1}\left(f'^2 - \varepsilon^2\right) + \frac{\sigma_{nf}/\sigma_f}{\rho_{nf}/\rho_f}M\left(f' - \varepsilon\right) + \frac{\mu_{nf}/\mu_f}{\rho_{nf}/\rho_f}\lambda\left(f' - \varepsilon\right) + \frac{1}{\rho_{nf}/\rho_f}Fr(f'^2 - \varepsilon^2)\right)$$
$$f'(4) = f(5)$$
$$f'(5) = -\frac{Pr}{\left(\frac{k_{nf}}{k_f} + \frac{4}{3}Rd\right)}\left(\frac{(\rho C_p)_{nf}}{(\rho C_p)_f}f\theta' + \frac{\mu_{nf}}{\mu_f}Ecf''^2\right)$$

Step III: The boundary conditions have been transformed in accordance with the new variables as:

$$fa(1) = \alpha\left(\frac{1-m}{1+m}\right),\ fa(2) = 1,\ fa(4) = 1,\ fb(2) = \varepsilon,\ fa(4) = 0.$$

Here, fa designate position at $\eta = 0$ and fb designate position as $\eta \to \infty$.

Step IV: Further, we use the bvp4c solver in MATLAB software to solve the entity of first-degree equations together with boundary conditions. For the first iteration of the solution, we offered an initial guess as well as a mesh size of 0.01.

3 Results and Discussion

The main purpose of this section is to interpret the velocity and temperature distribution for the various values of the relevant parameters. The bvp4c approach will be employed to numerically solve the highly nonlinear coupled Equations (14) and (15), along with the boundary condition (Equation (16)). To analyse the consequences of pertinent parameters, i.e. magnetic field parameter (M), porosity parameter (λ), Forchheimer parameter (Fr), stretching parameter (ε), radiation parameter (Rd), velocity power index (m), Prandtl number (Pr), wall thickness parameter (α), Eckert number (Ec), solid volume fraction (ϕ), tables and graphs have been represented. For obtaining the results, we have considered the parameters as $m = 0.5$, $Rd = 0.1$, $\alpha = 0.5$, $Pr = 6.2$, $Ec = 0.1$, $M = 1.0$, $\varepsilon = 0.01$, $\lambda = 0.1$, $Fr = 0.1$, $\phi = 0.1$, unless otherwise stated. Tables 1 and 2 represent the thermophysical terrain of magnetic nanoparticles along with base fluids and nanofluid respectively. Table 3 displays a comparative study of $-f''(0)$ for different values of m & α with $Rd = Ec = M = S = \alpha = \lambda = Fr = \phi = 0$ at $Pr = 6.2$ in the present work & those work obtained prior by[22]. The values so attained in existing study are in good agreement with the already-published ones. Table 4 displays the variation of coefficient of Skin friction and local Nusselt numbers in relation to power law index (m), stretching parameter (ε), magnetic parameter (M), porosity parameter (λ), Forchhiemer parameter (Fr), solid-volume fraction (ϕ), Prandtl number (Pr), wall thickness parameter (α), Eckert number (Ec), and radiation parameter (Rd) respectively. In this table, the numerical values of coefficient of local Skin friction and the coefficient of local Nusselt numbers are displayed. It is noted that the coefficient of local Skin friction escalates by boosting ε while it declines for decreasing values of m, M, λ, Fr, ϕ, α. Whereas the local Nusselt number escalates for rising values of ε, α, Pr, Rd and is declining for the decreasing values of m, M, λ, Fr, ϕ, and Ec.

Table 3. A Comparative study of $-f''(0)$ for distinct values of m for $\alpha = 0.25$ and $\alpha = 0.5$ where $Pr = 6.2$

Continued on next page

Table 3 continued

	Archie et al. [22]		Present Results		% of error	
m	$\alpha = 0.25$	$\alpha = 0.5$	$\alpha = 0.25$	$\alpha = 0.5$	$\alpha = 0.25$	$\alpha = 0.5$
10	1.1433	1.0603	1.1433	1.0603	0	0
9	1.1404	1.0589	1.1404	1.0589	0	0
7	1.1323	1.0551	1.1323	1.0551	0	0
5	1.1186	1.0486	1.1186	1.0486	0	0
3	1.0905	1.0359	1.0905	1.0359	0	0
1	1.0000	1.0000	1.0000	1.0000	0	0
0.5	0.9338	0.9799	0.9338	0.9799	0	0
0	0.7843	0.9576	0.7842	0.9576	0.0127	0
-1/3	0.5000	1.0000	0.5000	1.0000	0	0
-0.5	0.0833	1.1667	0.08333	1.1667	0	0
-0.55	-0.1976	1.2807	-0.1976	1.2807	0	0

Table 4. Numerical results of the Skin friction coefficient & Nusselt number for the current study when $Pr = 6.2$

m	M	λ	Fr	ε	ϕ	α	Pr	Ec	Rd	$\frac{\mu_{hnf}}{\mu_f}\sqrt{\frac{m+1}{2}}\,f''(\eta)$	$-\left(\frac{k_{hnf}}{k_f}+\frac{4}{3}\mathbf{Rd}\right)\sqrt{\frac{m+1}{2}}\,\theta'(\eta)$
0.5	1.0	0.1	0.1	0.01	0.1	0.5	6.2	0.1	0.1	-1.7005	1.8429
0.1										-1.4840	2.4164
0.2										-1.5395	2.2419
0.3										-1.5943	2.0909
0.4										-1.6480	1.9590
	0.5									-1.4880	1.9468
	1.0									-1.7005	1.8429
	1.5									-1.8883	1.7508
	2.0									-2.0583	1.6675
		0.1								-1.7005	1.8429
		0.2								-1.7389	1.8241
		0.3								-1.7763	1.8058
		0.4								-1.8130	1.7878
			0.1							-1.7005	1.8429
			0.2							-1.7199	1.8362
			0.3							-1.7390	1.8295
			0.4							-1.7579	1.8230
				0.5						-0.9774	2.3215
				1.0						-2.0911	2.6141
				1.5						1.1790	2.6223
				2.0						2.5336	2.2778
					0.05					-1.4764	1.8535
					0.10					-1.7005	1.8429
					0.15					-1.9535	1.8280
					0.20					-2.2429	1.8078
						0.0				-1.5943	1.2669
						0.25				-1.6466	1.5466
						0.50				-1.7005	1.8429
						0.75				-1.7560	2.1537
							3.0			-1.7005	1.1127
							5.0			-1.7005	1.5906
							7.0			-1.7005	2.0016
							10.0			-1.7005	2.5491
								0.1		-1.7005	1.8429
								0.2		-1.7005	1.4176
								0.3		-1.7005	0.9923
								0.4		-1.7005	0.5670
									0.0	-1.7005	1.7852

Continued on next page

Table 4 continued

0.5	-1.7005	2.0386
1.0	-1.7005	2.2282
1.5	-1.7005	2.3783

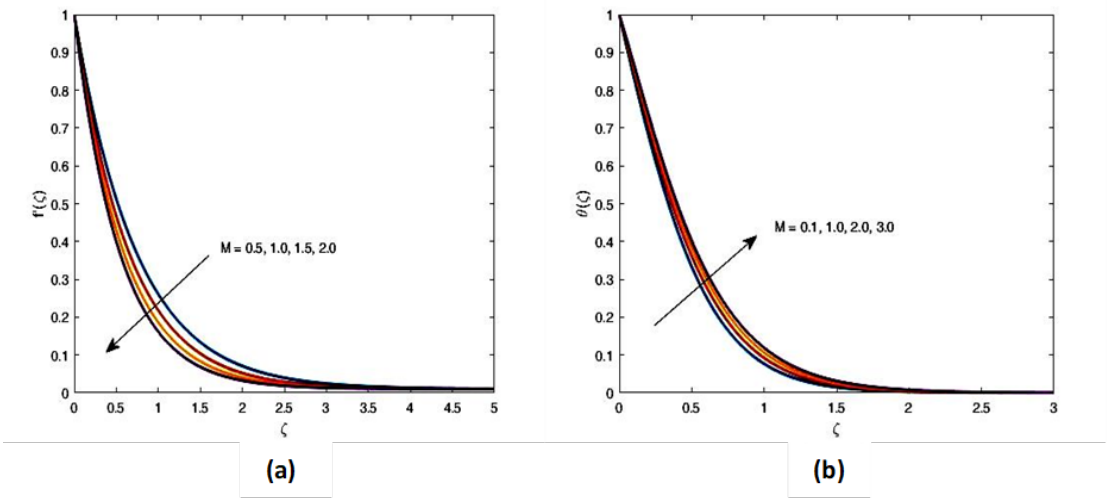

Fig 2. Effect of Magnetic Parameter (M) **on** $f^{'}(\zeta)$ *and* $\theta(\zeta)$

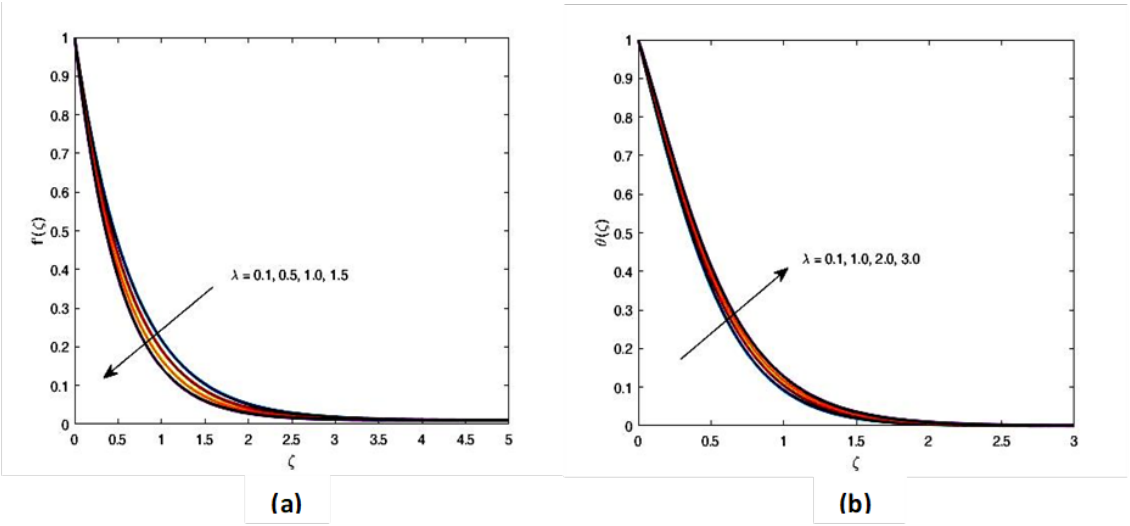

Fig 3. Effect of Porosity parameter (λ)**on** $f'(\zeta)$ *and* $\theta(\zeta)$

Figure 2**(a)** demonstrates that the nanofluid's velocity decreases in accordance with the magnetic field parameter (M). Because of this, the boundary layer thickness that governs velocity diminishes. Substantially, this is reliable because Lorentz force, which is retarding in nature and proves the existence of a magnetic field in an electrically conductive nanofluid, tends to slow down the fluid's velocity. Figure 2**(b)** depicts the introduction of a horizontal magnetic field that results in Lorentz force, a resistive force that causes fluid resistance to increase by increasing friction throughout its layers, and this result is in good agreement with [19]. Figure 3**(a)-(b)** display the impacts of the porosity parameter (λ) on velocity and temperature profiles. It can be noticed that the velocity of the fluid decreases as the porous medium is to raise the hindrance to fluid motion, whereas an adverse effect is seen for the temperature profile along with the increasing values of the porosity parameter. Figure 4**(a)-(b)** show

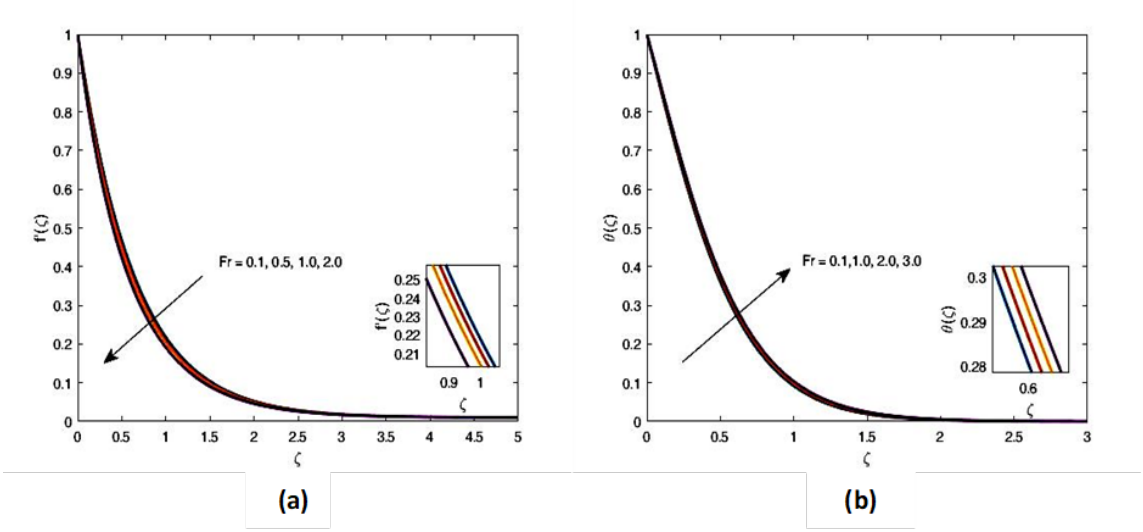

Fig 4. Effect of Forchheimer number (*Fr*) on $f'(\zeta)$ *and* $\theta(\zeta)$

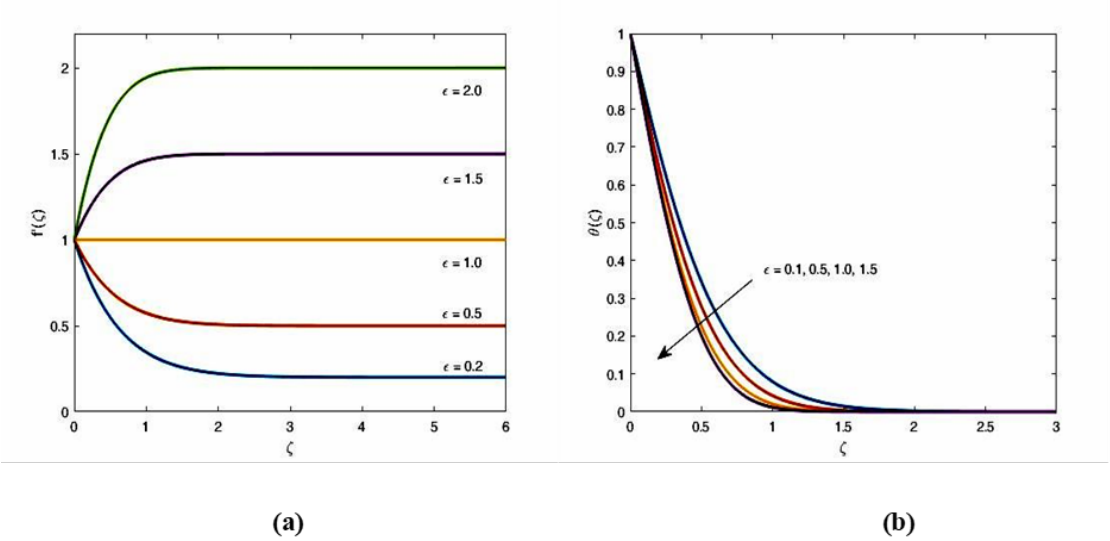

Fig 5. Effect of Stretching Parameter $(\in)$ **on** $f'(\zeta)$ *and* $\theta(\zeta)$

the effects of the local Forchheimer number (Fr) (inertia coefficient). It is clear from the figure that the inertia coefficient has a negative impact on fluid velocity since it is inversely proportional to the permeability of the medium and the drag coefficient. Therefore, with increasing values of Cb, the permeability of the medium & drag coefficient both rise. As a result, the frictional force for the liquid is improved, resulting in decreased velocity and a bigger Forchheimer number, however, the temperature profile exhibits the reverse tendency as the Forchheimer parameter increases and this result is in good agreement with [22]. The impact of velocity ratio parameter (ε) upon the velocity profile is depicted in Figure 5**(a)**. In case, when the pace of free flow is larger than the stretched sheet's pace, it is evident that when ε is increased, the velocity boosted as well as associated boundary layer thickness declines. The stretching action near a stagnant area expands, causing the external free flow to accelerate and the velocity to rise. Whenever, the velocity of sheet surpasses the velocity of free stream, the velocity & associated boundary layer thickness both expanding. Furthermore, the boundary layer is not produced at $\varepsilon = 1$. Temperature profile declines with an increase in ε, as depicted in Figure 5**(b)**, which displays the temperature profile that exhibits the opposite behaviour. The impacts of Prandtl number (Pr), Eckert number (Ec), & radiation parameter (Rd) upon temperature profiles are portrayed in

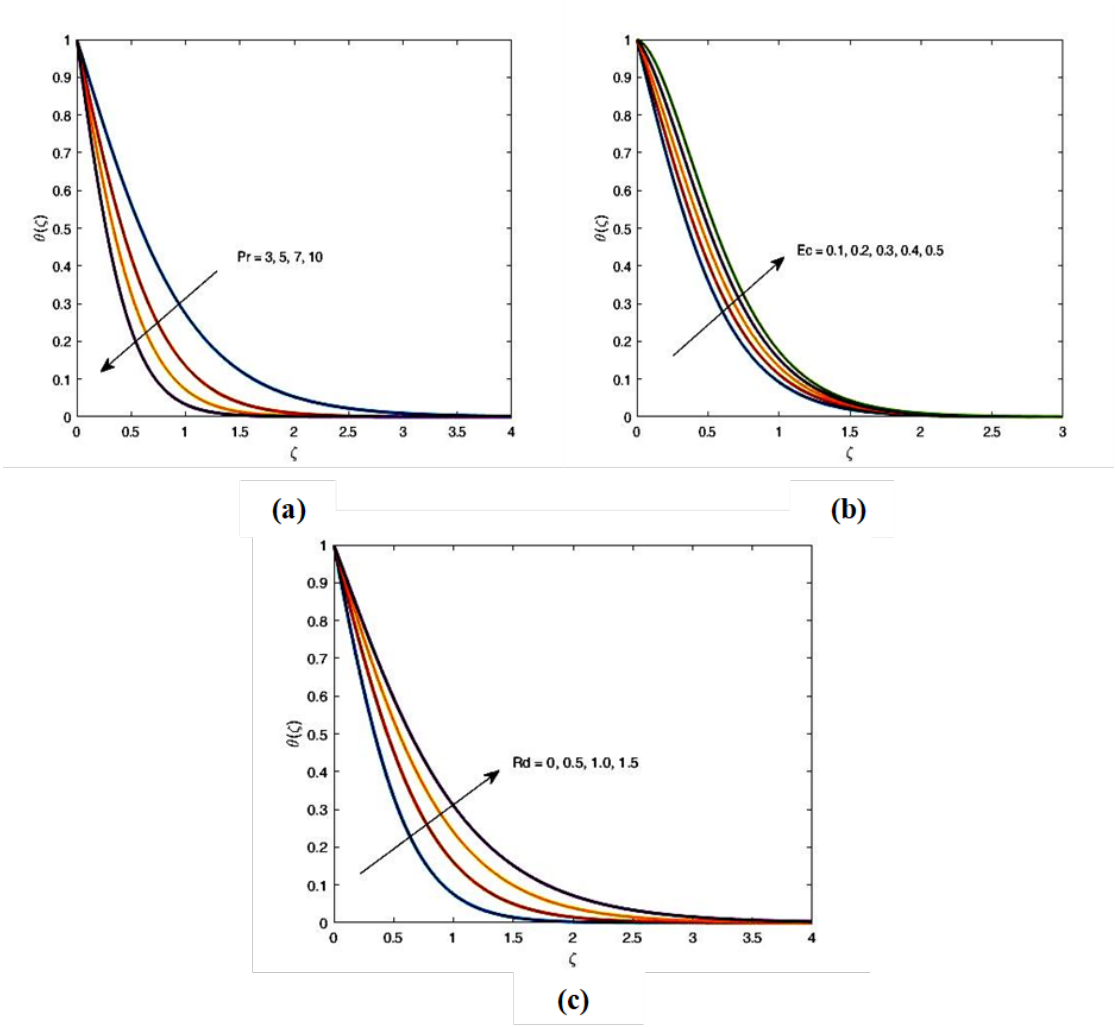

Fig 6. Effect of Prandtl number (*Pr*) on $f'(\zeta)$Eckert number (Ec) and Radiation parameter (Rd) on $\theta(\zeta)$

Figure 6**(a)**-**(c)** accordingly. Figure 6**(a)** illustrates how the Prandtl number (*Pr*) had an impact on temperature distribution. A material quality that differs from fluid to fluid corresponds to the Prandtl number. The figure shows that fluid temperature drops as *Pr* rises. It is implied that momentum diffusivity has a larger value than thermal diffusivity for large *Pr*. As a result, the thickness of energy boundary layer reduces. Usually, *Pr* is used in heat transfer problems for lowering the allied thickness of both thermal and momentum boundary layers and has good agreement with [19]. The temperature profiles are enhanced by an escalation in either Eckert number or radiation parameter, as seen in Figure 6**(b)**-**(c)**. Figure 6**(b)** signifies the effects of Eckert number (Ec) on temperature profile. The results of Eckert number coincide with the Ajayi et al. [23]. It is seen that for larger values of the Eckert number parameter intensifies (improves) the thermal boundary layer thickness. Generally, the rising values of Eckert number encourages the diffusion of particles due to this cause we saw improvement in thermal boundary layers. Figure 6 **(c)** shows the effect of thermal radiation on temperature profile $\theta(\zeta)$. It is found that radiation provides an enhancement on the fluid temperature. The rate of heat transfer at the surface reduces for higher thermal radiation effects. Higher temperature and thicker thermal boundary layer thickness associated with larger radiation parameter. Higher values of radiation parameter lead to a low rate of heat transfer at the surface because the nanofluid temperature is enhanced.

4 Conclusion

This work examined the impacts of thermal radiation and viscous dissipation on the MHD outflow of magnetic nanofluid Fe_3O_4/H_2O past stretching sheet with variable thickness utilising the Darcy-Forchheimer model in porous medium. Taking

into account thermal radiation and viscous dissipation in magnetic nanoparticle flow makes temperature control better. This makes medical uses like targeted drug delivery and hyperthermia treatment better, especially in cancer therapy. **Scope:** An expansion of the scope of thermal radiation and viscous dissipation that incorporates MNPs might result in breakthroughs in data storage and sensing technologies as well as environmental applications, such as the removal of pollutants and the purification of water. Continued research and development are key to unlocking the full range of possibilities for magnetic nanoparticles in diverse fields. The main outcomes of the current investigation can be listed below:

- An augmentation in values of porosity parameter (λ), magnetic field (M), Forchheimer number (Fr) reduces the momentum boundary layer thickness although increases the thermal boundary layer thickness.
- An increase in the fluid's temperature is due to an increase either in radiation parameter (Rd) or in the Eckert number (Ec).
- Escalation in Prandtl number (Pr) lowers the compactness of thermal boundary layer.
- An augmentation in any of the values of magnetic field (M), velocity power index (m), forchheimer number (Fr), porosity parameter (λ), wall thickness parameter (α) exalts frictional factor whilst the frictional factor upsurges with stretching parameter (ε).
- An increase in any of the parameters such as magnetic field(M), porosity parameter (λ), velocity power index (m), forchheimer number (Fr), Eckert number (Ec) can reduce the Nusselt number while it enhances for stretching parameter (ε), wall thickness parameter (α), radiation parameter (Rd), Prandtl number (Pr).

5 Nomenclature

BVP - Boundary value problem; ODE - Ordinary differential equation ; PDE - Partial differential equation; MHD - Magnetohydrodynamics; η - Dimensionless variable , f - Dimensionless stream function; θ - Dimensionless temperature function; ζ - Modified dimensionless variable; C_{fx} - Skin friction coefficient; Nu_x - Nusselt number; Re_x - Reynold's number; M - Magnetic parameter; λ - Porosity parameter; Fr - Forcheimmer number ; ε - Velocity ratio parameter; ϕ - Dimensionless concentration function; Pr - Prandtl's number; Ec - Eckert number; Rd - Radiation paramter; α - Thermal diffusivity; m - Velocity power index; k - Thermal conductivity; μ - Dynamic viscosity; ν - Kinematic viscosity; ρ - Density; σ - Electrical conductivity; C_p - Specific heat at constant pressure; σ^* - Stefan-Boltzman constant; K^* - Mean absorption co-efficient; τ_w - Shear stress at the wall; q_w - Heat flux; T - Absolute free temp. of the fluid; T_w - The temp. of the stretching surface; T_∞ - The temp. of the free stream; U_w - The stretching velocity at surface; U_∞ - Free stream velocity of the fluid; u, v - Horizontal and vertical velocity comp; x, y - Cartesian coordinates

References

1) Alabdulhadi S, Bakar SA, Ishak A, Waini I, Ahmed SE. Effect of Buoyancy Force on an Unsteady Thin Film Flow of Al2O3/Water Nanofluid over an Inclined Stretching Sheet. *Mathematics*. 2023;11(3):1–16. Available from: https://doi.org/10.3390/math11030739.
2) Zeb H, Wahab HA, Khan U, Juhani ASA, Andualem M, Khan I. The Velocity Slip Boundary Condition Effects on Non-Newtonian Ferrofluid over a Stretching Sheet. *Mathematical Problems in Engineering*. 2022;2022:1–20. Available from: https://doi.org/10.1155/2022/1243333.
3) Abbas Z, Mushtaq T, Shehzad SA, Rauf A, Kumar R. Slip flow of hydromagnetic micropolar nanofluid between two disks with characterization of porous medium. *Journal of the Brazilian Society of Mechanical Sciences and Engineering*. 2019;41(10):1–3. Available from: https://doi.org/10.1007/s40430-019-1974-6.
4) Rauf A, Shehzad SA, Abbas Z, Hayat T. Unsteady three-dimensional MHD flow of the micropolar fluid over an oscillatory disk with Cattaneo-Christov double diffusion. *Applied Mathematics and Mechanics*. 2019;40(10):1471–1486. Available from: https://doi.org/10.1007/s10483-019-2530-6.
5) Ullah Z, Abbas A, El-Zahar ER, Seddek LF, Akgul A, Hassan AM. Significance of thermal density and viscous dissipation on heat and mass transfer of chemically reactive nanofluid flow along stretching sheet under magnetic field. *Results in Engineering*. 2023;20:1–12. Available from: https://doi.org/10.1016/j.rineng.2023.101413.
6) Shah SAGA, Hassan A, Karamti H, Alhushaybari A, Eldin SM, Galal AM. Effect of thermal radiation on convective heat transfer in MHD boundary layer Carreau fluid with chemical reaction. *Scientific Reports*. 2023;13(1):1–11. Available from: https://doi.org/10.1038/s41598-023-31151-4.
7) Umavathi JC, Hemavathi K. Flow and heat transfer of composite porous medium saturated with nanofluid. *Propulsion and Power Research*. 2019;8(2):173–181. Available from: https://doi.org/10.1016/j.jppr.2019.01.010.
8) Aleem M, Asjad MI, Shaheen A, Khan I. MHD Influence on different water based nanofluids (TiO2, Al2O3, CuO) in porous medium with chemical reaction and newtonian heating. *Chaos, Solitons & Fractals*. 2020;130:109437. Available from: https://doi.org/10.1016/j.chaos.2019.109437.
9) Bejawada SG, Reddy YD, Jamshed W, Nisar KS, Alharbi AN, Chouikh R. Radiation effect on MHD Casson fluid flow over an inclined non-linear surface with chemical reaction in a Forchheimer porous medium. *Alexandria Engineering Journal*. 2022;61(10):8207–8220. Available from: https://doi.org/10.1016/j.aej.2022.01.043.
10) Hussain M, Sheremet M. Convection analysis of the radiative nanofluid flow through porous media over a stretching surface with inclined magnetic field. *International Communications in Heat and Mass Transfer*. 2023;140:106559. Available from: https://doi.org/10.1016/j.icheatmasstransfer.2022.106559.
11) Awais M, Salahuddin T, Muhammad S. Effects of viscous dissipation and activation energy for the MHD Eyring-powell fluid flow with Darcy-Forchheimer and variable fluid properties. *Ain Shams Engineering Journal*. 2024;15(2):1–15. Available from: https://doi.org/10.1016/j.asej.2023.102422.

12) Khashi'ie NS, Waini I, Kasim ARM, Zainal NA, Ishak A, Pop I. Magnetohydrodynamic and viscous dissipation effects on radiative heat transfer of non-Newtonian fluid flow past a nonlinearly shrinking sheet: Reiner–Philippoff model. *Alexandria Engineering Journal*. 2022;61(10):7605–7617. Available from: https://doi.org/10.1016/j.aej.2022.01.014.
13) Saidulu B, Reddy KS. Evaluation of combined heat and mass transfer in hydromagnetic micropolar flow along a stretching sheet when viscous dissipation and chemical reaction is present. *Partial Differential Equations in Applied Mathematics*. 2023;7:1–8. Available from: https://doi.org/10.1016/j.padiff.2022.100467.
14) Sharma RP, Acharya N, Das K. On the impact of variable thickness and melting transfer of heat on magnetohydrodynamics nanofluid flow past a slendering stretching sheet. *Indian Journal of Geo Marine Sciences*. 2020;49(4):641–648. Available from: http://nopr.niscpr.res.in/handle/123456789/54647.
15) Dharmaiah G, Mebarek-Oudina F, Kumar MS, Kala KC. Nuclear reactor application on Jeffrey fluid flow with Falkner-skan factor, Brownian and thermophoresis, non linear thermal radiation impacts past a wedge. *Journal of the Indian Chemical Society*. 2023;100(2):100907. Available from: https://doi.org/10.1016/j.jics.2023.100907.
16) Irfan M, Farooq MA, Iqra T. A New Computational Technique Design for EMHD Nanofluid Flow Over a Variable Thickness Surface With Variable Liquid Characteristics. *Frontiers in Physics*. 2020;8:1–14. Available from: https://doi.org/10.3389/fphy.2020.00066.
17) Seth GS, Mandal PK. Analysis of Electromagnetohydrodynamic Stagnation Point Flow of Nanofluid Over a Nonlinear Stretching Sheet with Variable Thickness. *Journal of Mechanics*. 2019;35(5):719–733. Available from: https://doi.org/10.1017/jmech.2019.2.
18) Abderrahmane A, Mourad A, Mohammed S, Smaisim GF, Toghraie D, Koulali A, et al. Second law analysis of a 3D magnetic buoyancy-driven flow of hybrid nanofluid inside a wavy cubical cavity partially filled with porous layer and non-Newtonian layer. *Annals of Nuclear Energy*. 2023;181:109511. Available from: https://doi.org/10.1016/j.anucene.2022.109511.
19) Sharma S. MHD Boundary Layer Flow Past an Exponentially Stretching Sheet with Darcy-Forchheimer Flow of Nanofluids. *Indian Journal Of Science And Technology*. 2022;15(33):1594–1604. Available from: https://doi.org/10.17485/IJST/v15i33.607.
20) Kierzenka J, Shampine LF. A BVP solver based on residual control and the Maltab PSE. *ACM Transactions on Mathematical Software*. 2001;27(3):299–316. Available from: https://doi.org/10.1145/502800.502801.
21) Shampine LF. Singular boundary value problems for ODEs. *Applied Mathematics and Computation*. 2003;138(1):99–112. Available from: https://doi.org/10.1016/S0096-3003(02)00111-X.
22) Thakur A, Sood S. Tri-Hybrid Nanofluid Flow Towards Convectively Heated Stretching Riga Plate with Variable Thickness. *Journal of Nanofluids*. 2023;12(4):1129–1140. Available from: https://www.ingentaconnect.com/contentone/asp/jon/2023/00000012/00000004/art00022?crawler=true&mimetype=application/pdf.
23) Ajayi TM, Omowaye AJ, Animasaun IL. Viscous Dissipation Effects on the Motion of Casson Fluid over an Upper Horizontal Thermally Stratified Melting Surface of a Paraboloid of Revolution: Boundary Layer Analysis. *Journal of Applied Mathematics*. 2017;2017:1–13. Available from: https://doi.org/10.1155/2017/1697135.